

УДК 539.1.07

INVESTIGATION OF THE CHARGE COLLECTION FOR STRONGLY IRRADIATED SILICON STRIP DETECTORS OF THE CMS ECAL PRESHOWER

*Ph.Bloch^a, A.Peisert^a, Y.H.Chang^b, A.E.Chen^b, S.Hou^b, W.T.Lin^b,
A.E.Chermukhin^c, I.A.Golutvin^c, A.R.Urkinbaev^{c1}, N.I.Zamiatin^c, D.Loukas^d*

^aCERN, Geneva

^bNational Central University, Chungli, Taiwan

^cJoint Institute for Nuclear Research, Dubna

^dInstitute of Nuclear Physics «Demokritos», Attiki, Greece

Strongly irradiated ($2.3 \cdot 10^{14}$ n/cm²) silicon strip detectors of different size, thickness and different design options were tested in a muon beam at CERN in 1999. A charge collection efficiency in excess of 85 % and a signal-to-noise ratio of about 6 are obtained in all cases at high enough bias voltage. Details of the charge collection in the interstrip and the guard ring region and cross-talk between strips were also studied. We find that the charge collection efficiency and the cross-talk between strips depend on the interstrip distance.

В 1999 году на мюонном пучке установки SPS CERN были проведены испытания сильно облученных ($2,3 \cdot 10^{14}$ н/см²) стриповых кремниевых детекторов различного размера, толщины и с различными конструкционными особенностями. Для всех исследованных образцов получена эффективность сбора заряда выше 85 % и величина отношения сигнала к шуму около 6 при достаточно больших напряжениях смещения. Детально изучены сбор зарядов в межстриповых областях детекторов и в областях охранных колец, проблема «cross-talk» между стрипами. Установлено, что эффективность сбора зарядов в детекторах и величина «cross-talk» между стрипами зависят от расстояния между стрипами.

INTRODUCTION

The expected high hadron fluence in the silicon strip detectors of the CMS Preshower detector requires careful design of the sensors. During and after irradiation, the sensors will suffer surface damage, bulk damage and changes of the doping concentration. The aim of the test in July 1999 using a precision telescope was to study the charge collection efficiency (CCE) for irradiated detectors of various topologies.

Many measurements on the charge collection of irradiated Preshower detectors have already been done in the laboratory using a ¹⁰⁶Ru radioactive source [1]. However the geometry and trigger conditions with the source are less precise than in a beam and do not allow us to study fine details such as the collection in the interstrip or the guard ring region. We have already shown with nonirradiated detectors that detailed studies can be performed in a high energy beam using a precise telescope [2].

Nine detectors were studied during the run in 1999; we present here the main results of this test.

¹On leave of absence from INP, Tashkent.

1. EXPERIMENTAL SET-UP DESCRIPTION

A schematic view of the experimental set-up is shown in Fig. 1. A beam telescope, provided by the Taiwanese group, consisting of 10 microstrip detectors read by a Viking chip [3], was inserted inside a commercial freezer. This telescope allowed one to reconstruct tracks in 2 dimensions with a precision of the order of 10 micrometers. Silicon Preshower detectors (at maximum 2 at a time) were inserted in the middle of the telescope.

These silicon detectors were read at 40 MHz sampling rate with the SCT32 [4] chip, connected through a discrete array of capacitances in order to cope with the large bulk current due to irradiation. The temperature regulation of the freezer was set to the minimum (-30°C) to reduce the leakage current and therefore maximise the signal-to-noise ratio. There was no active cooling (only the freezer convection), so the exact temperature of the detectors in presence of electronics was $\approx -20^{\circ}\text{C}$, but the leakage current was always very stable.

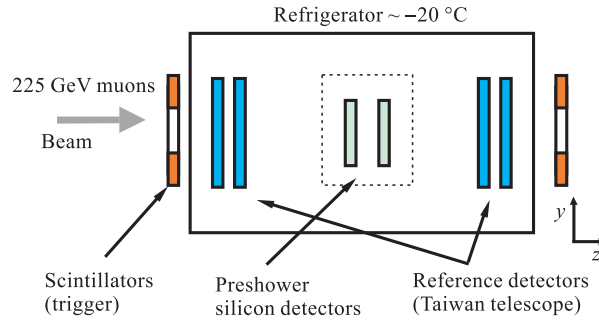


Fig. 1. Schematic of the experimental set-up

An 8 ns wide coincidence was required between the 40 MHz clock and the particle trigger provided by scintillators, in order to select particles with a well defined phase relative to the clock. A sketch of the read-out system is shown in Fig. 2. A pulse generator was used for calibration runs during periods without beam. The channel calibration of the SCT32 chip was done without disconnecting it from the silicon detector.

With the four scintillation counters it was possible to vary the beam spot at the face of the studied silicon sensors. We used:

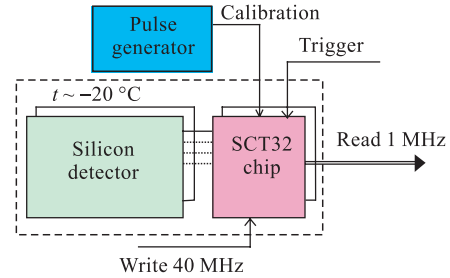


Fig. 2. Scheme of the read-out systems

- a 4-fold coincidence to select a small squared area ($\approx 10 \times 10$ mm),
- a 2-fold vertical coincidence to select a 30×10 mm area running along the strip length,
- a 2-fold horizontal coincidence to select a 10×30 mm area running across a large number of strips.

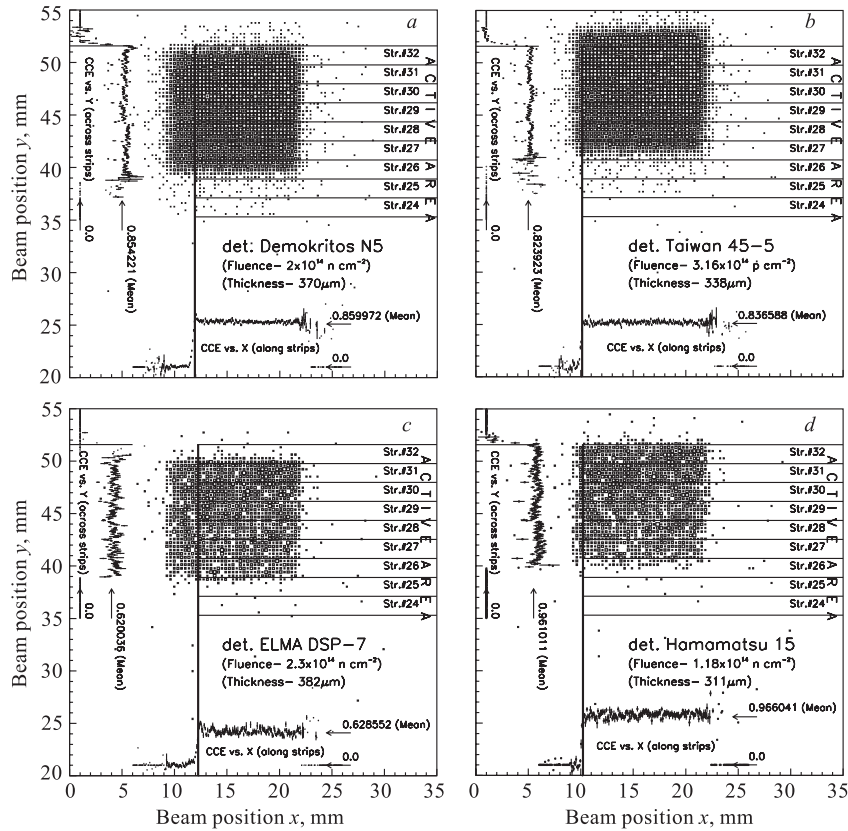


Fig. 3. Beam spot distributions and CCE distributions in two directions

In each case, the detectors were put in two different geometrical positions: either well centred on the beam or placed in such a way that the beam hit the last 6 strips and the corner of the detector. This last set of data can be used to study the charge collection close to the guard rings. Figure 3 shows the beam spot relative to the sensor active area for four such corner runs (for four detectors *a, b, c, d*, correspondingly). One sees that the beam spot did not always cover fully the detector corner so that the efficiency near the guard ring could in some cases only be studied in one direction (either *x* along the strips or *y* across the strips).

Data were taken parasitically to a CMS 225 GeV/c muon test run at the H2 area of the CERN SPS. About 2 million events were recorded, corresponding to 250 different conditions (various detectors, bias, positions).

2. SILICON-STRIP DETECTOR SAMPLES

Six sets of detectors were inserted in turn in the telescope. Unfortunately, the second read-out electronics card died slowly during the run so that the data of 3 detectors cannot be used. All except detector Hamamatsu 103 ($\rho = 0.9 \text{ k}\Omega \cdot \text{cm}$) have a resistivity higher than

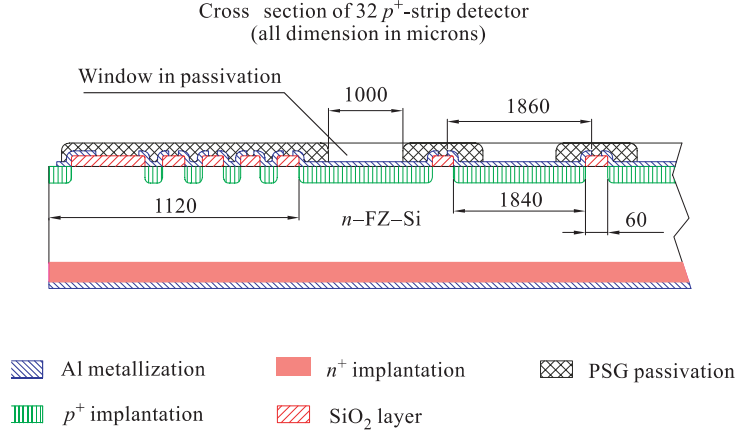


Fig. 4. A cross section of the silicon-strip detector

4 $\text{k}\Omega \cdot \text{cm}$. All the detectors had been pre-irradiated before, either at CERN-PS with 24 GeV protons or in Dubna [5] with fast neutrons, and kept at low temperature after irradiation (details on our irradiation facilities and procedures can be found in [1]).

The cross section of one of the detectors (Elma N9-1) is shown in Fig. 4. From left to right one sees the scribe line, four aluminized guard rings (GR) and the aluminized strips with a p^+ implant. Important parameters are the sensor thickness, the interstrip and the interimplant distances.

Table 1 summarizes the characteristics of each detector, as well as the fluence they received before the test and the full depletion voltage obtained from a CV curve at 5 kHz. The neutron fluences are expressed in «1 MeV neutron equivalent» unit. For the 24 GeV protons, we quote the received proton fluence: the «1 MeV neutron equivalent» fluence can be obtained by dividing it by a factor of approximately 2. The Taiwan and Takion detectors are multigeometry sensors with different interstrip distances.

Table 1. Main characteristics of tested detectors

Detector	Fluence, 10^{14} cm^{-2}	V_{fd} , V	Distance p^+ to p^+ , μm	Distance Al to Al, μm	Thickness, μm	Dimension, mm	Pitch size, mm
Hamamatsu 8	nonirradiated	60	110	70	313	60×60	1.81
Hamamatsu 15	1.18 n	149	110	70	311	60×60	1.81
Hamamatsu 103	0.96 n	32	110	70	322	60×60	1.81
DSP 7 (Elma)	2.30 n	509	120	80	382	60×60	1.81
D2-1- n^+ (Elma)	1.18 n	133	120	80	308	60×60	1.81
Taiwan 45-5	3.16 p	241	50	40	338	60×60	1.81
			160	150			
Takion-3	2.10 n	320	the same as previous		320	60×60	1.81
N9-1 (Elma)	3.16 p	214	60	40	300	63×63	1.90
N5 (Demokritos)	2.00 n	431	160	160	370	60×60	1.81

3. TEST PULSE CALIBRATION

For each detector, data were recorded with a calibrated pulse injection at a high enough bias voltage to be fully depleted. The timing of the test pulse was varied by steps of 12.5 ns, and the calibration is obtained from the highest signal observed. An attempt was also made to fit the shape of the pulse with a function of the form

$$f(t) = (b(t - t_0))^{a-1} e^{-b(t-t_0)}$$

and to take the function maximum: the results are similar within a few percents but somewhat less reliable. The injected charge was nominally 6.8 fC (68 mV on 0.1 pF). Since a minimum ionizing particle should deposit 4 fC in a 300 μm thick detector, we arbitrarily divide the calibration charge by a factor 1.7 to express our results in mip (minimum ionizing particle). The value of the injection capacitor (directly on chip) is known to be uniform between channels, but its absolute value may vary from one ASIC production to the next. Our normalization may therefore be simply wrong by 20 %. To overcome this difficulty, we have also measured a nonirradiated detector, and we determine an overall factor (later applied to all the data) in order to get exactly 1 mip for the nonirradiated detector at high bias (500 V).

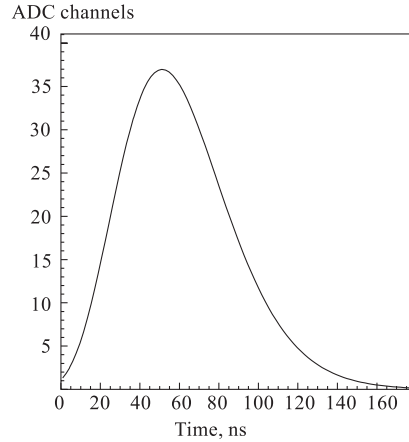


Fig. 5. Output pulse produced by a step-like injection charge

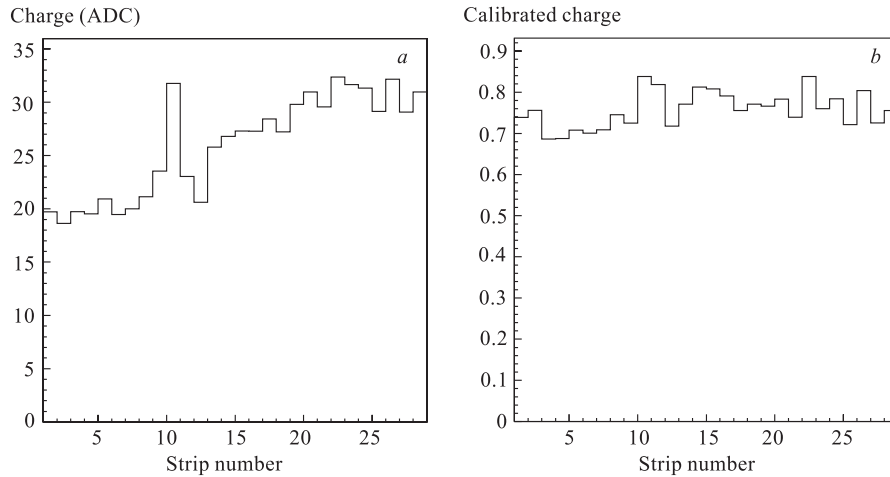


Fig. 6. Muon signal as a function of the strip number: *a*) before calibration; *b*) after calibration

Figure 5 shows a typical output pulse produced by a step-like injection charge. The pulse varies by less than $\sim 3\%$ when one moves by ± 6 ns around the maximum, showing that we are not sensitive to the remaining timing jitter between the clock and the trigger. Figure

6, *a,b* shows the effect of the calibration for data taken with one of the card (SCT2) which was particularly nonuniform¹: after calibration, the response is uniform with a dispersion of less than 5 %.

4. ALIGNMENT OF THE DETECTORS RELATIVE TO TELESCOPE

The alignment of the detectors relative to the telescope is determined using a simple technique: in each event, for each Preshower detector, we select the strip with the highest charge and we plot the difference between the y coordinate (as measured from the telescope) and the position of the centre of the strip (as defined in the local coordinate of the Preshower silicon detector). The resulting distribution is shown in Fig. 7. We observe a nice rectangle with almost no background on the 2 sides, which has the width of one strip. The sharp edges of the distribution can be fitted with a step function, and the strip centre is defined as the mean of the position of the 2 edges. The pitch of the strips is known very precisely.

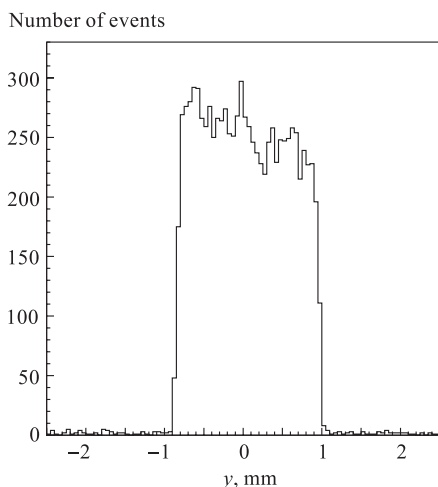


Fig. 7. Telescope y coordinate for events hitting a given preshower strip

A single translation constant can be used for each detector. The position along the beam is optimized in order to have the same alignment constant for tracks with various slopes dy/dz (z being along the beam). Finally, a possible rotation in the $x - y$ plane is evaluated by redoing the alignment for different values of the telescope x coordinate. By fitting the slope of the edges of the distribution after alignment, one can estimate the overall geometrical precision. This is a pessimistic estimate, because the sharpness of the edges may be smeared by other physical effects than the position resolution, for example by the charge sharing between strip implants. Nevertheless, in all the cases, we find a precision better than $16 \mu\text{m}$.

5. DATA ANALYSIS

Before detailed analysis, the data are processed through the following steps:

1. Pedestal computation. In an event, very few strips have a charge signal. The plot of the raw charge distribution exhibits therefore a large peak at zero charge which is fitted by a Gaussian curve to determine both the pedestal position and the noise for each individual run.
2. Common noise subtraction. The data suffer from low frequency external noise. This «common» noise (CN) can be easily removed event by event by identifying strips

¹This nonuniformity is a known defect of SCT32 and has been corrected in later versions such as the SCT 128.

6. CHARGE COLLECTION EFFICIENCY VERSUS BIAS VOLTAGE

6.1. Analysis in Stand-Alone Mode. The first analysis was performed in September 1999 before the telescope data were available. The Preshower silicon detector was scanned and the charge of the highest strip was retained as signal. The common noise subtraction was done using 5-strips wide regions. From the results on cross-talk presented in Section 7, it appears that this may have resulted in a slight underestimate of the charge, since the 2 neighbour strips have often been used for common noise subtraction. But the effect should be very small (maximum 2.5 %) and was the same for the reference detector. The most probable value of the charge distribution was determined using a local Gaussian fit.

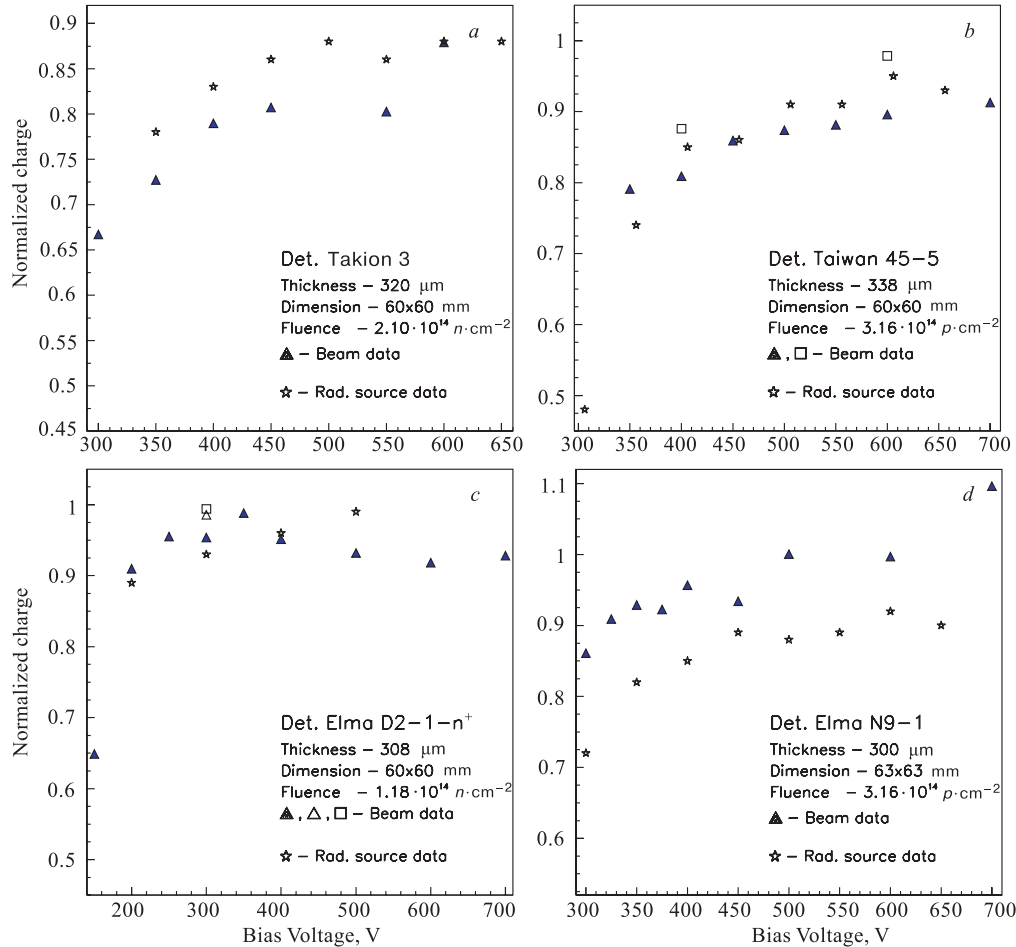


Fig. 10. Normalized charge for the detectors Takion 3 (a), Taiwan 45-5 (b), Elma D2-1-n⁺ (c), Elma N9-1 (d)

Figure 8 shows the most probable value of the charge distribution for the nonirradiated (reference) detector Hamamatsu 8 as a function of the bias voltage. An overall normalization factor has been applied to obtain charge unity at $V = 500 \text{ V}$. The detector shows a full

charge collection around 80 V. Note that the reference data of Hamamatsu 8 had been taken without making a coincidence between trigger and clock, so that the arrival of the particle was random relative to the 40 MHz clock. A cut has been applied on the ratio of the first to second time sample to ensure a good timing. The result of a run taken at a later stage with a proper timing is also shown on Fig. 8 and is in good agreement.

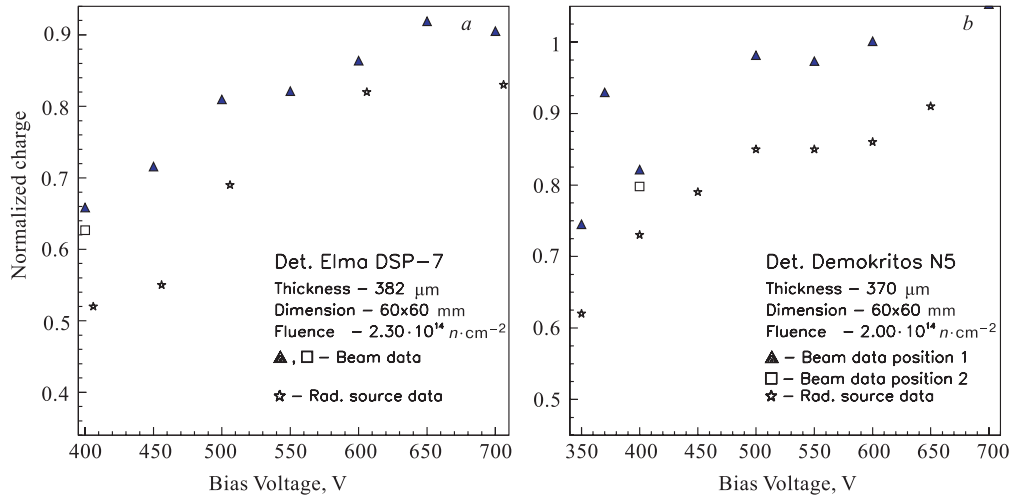


Fig. 11. Normalized charge for the detectors Elma DSP7 (a) and Demokritos N5 (b)

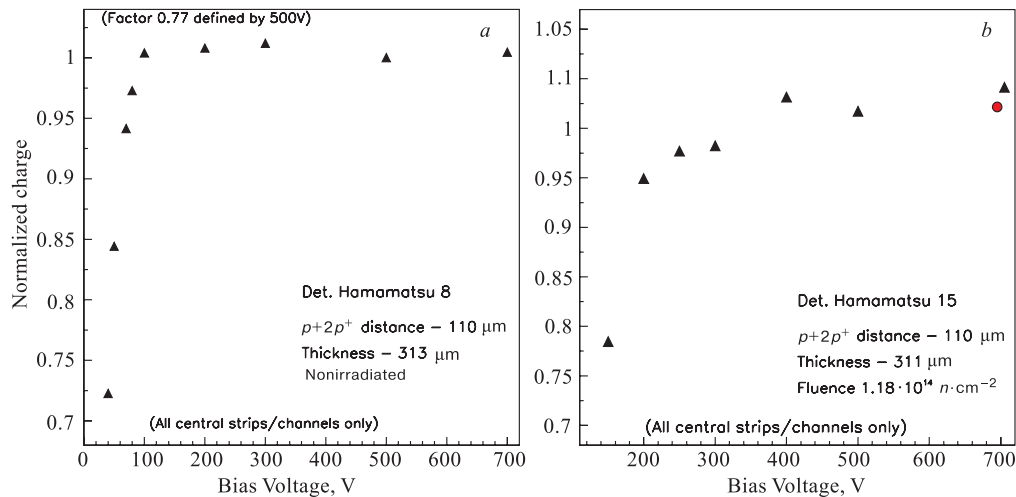


Fig. 12. Normalized charges for the detectors (with telescope) Hamamatsu 8 (a) and Hamamatsu 15 (b)

The same procedure was subsequently applied to all other detectors. The measured charge has been corrected for calibration, the overall normalization factor applied and finally the

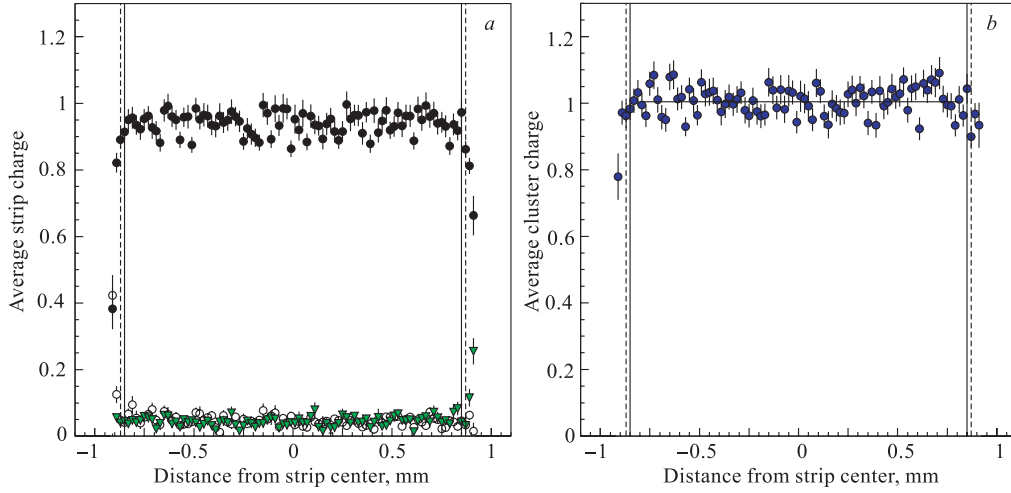


Fig. 13. Average normalized strip charges (*a*) and normalized cluster (*b*) as a function of the distance to the center of the central strip for Hamamatsu 8 at 100 V

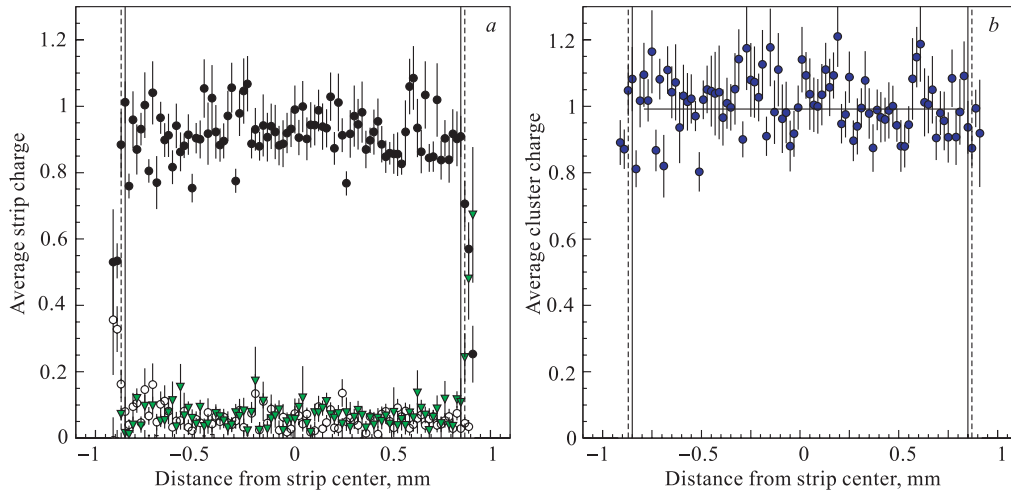


Fig. 14. Average strip (*a*) and cluster (*b*) charges as a function of the distance to the center of the central strip for Hamamatsu 15 at 700 V

charge has been normalized to the thickness of Hamamatsu 8 ($313 \mu\text{m}$). Figures 9, 10, *a,b,c,d* show the measurements obtained for the thin ($\sim 300 \mu\text{m}$) detectors. The charge collection efficiency measured in the laboratory with the ^{106}Ru source is also shown. The shapes are in excellent agreement. The absolute values differ slightly, but we could not find any systematic deviation: the difference of efficiency on the plateau between the beam and the source measurement for the five plots of Figs. 9,10 has a dispersion of 5 %, which we consider as a reasonable estimate of the uncertainty in the whole normalization procedure.

Figures 11, *a,b* show the charge collection efficiency for the 2 detectors which have a large thickness. It is clear that for heavily irradiated fat detectors, the efficiency plateau is difficult to reach. Surprisingly, there is in these 2 cases a bigger disagreement between the source and the beam normalization (the results with the beam look too high), but the shapes still agree very well.

6.2. Analysis Using the Telescope. All runs were later reanalysed using the telescope to define which strip should be used for the charge measurement. This method allows us to remove events with poor tracks or tracks outside the fiducial area. The rest of the procedure is identical as before. There is a good agreement between the two analyses. (compare Fig. 12, *a,b* with Fig. 8 and Fig. 9, respectively).

6.3. Conclusions on Charge Collection vs. Bias. The measurements done with the beam confirm the results obtained in the laboratory with a simpler set-up using a radioactive source. A good plateau with an efficiency $> 85\%$ is always obtained for thin irradiated detectors.

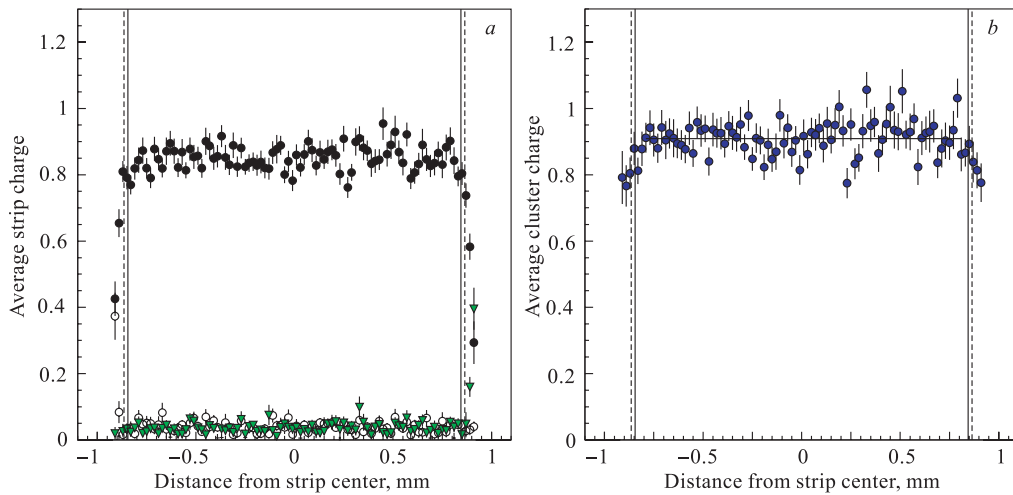


Fig. 15. Average strip (*a*) and cluster (*b*) charges as a function of the distance to the center of the central strip for D2-1-n⁺ at 300 V

7. ANALYSIS OF THE CHARGE IN THE CENTRAL AND NEIGHBOURING STRIPS AS A FUNCTION OF PARTICLE POSITION

7.1. Study of Inter-Strip Region. In this analysis the central strip is defined as the strip which should be hit according to the telescope measurement. Figures 13–16 show the average value of the charge measured in the central strip and its two neighbours as a function of the track position for a few detectors, in steps of 20 microns. The average charge is computed in the interval from -1 and $+3$ normalized charges, to avoid fluctuations due to the long Landau tail. In each case we present two plots. The plot on the left shows the charge in the central strip (black dots), the charge of the strip on the left (open circles) and on the right (full triangles). The solid (respectively dashed) line shows the area covered by the p^+

implant (respectively the aluminization). The right plot shows the total charge of the «cluster» (summing the charge of 3 strips).

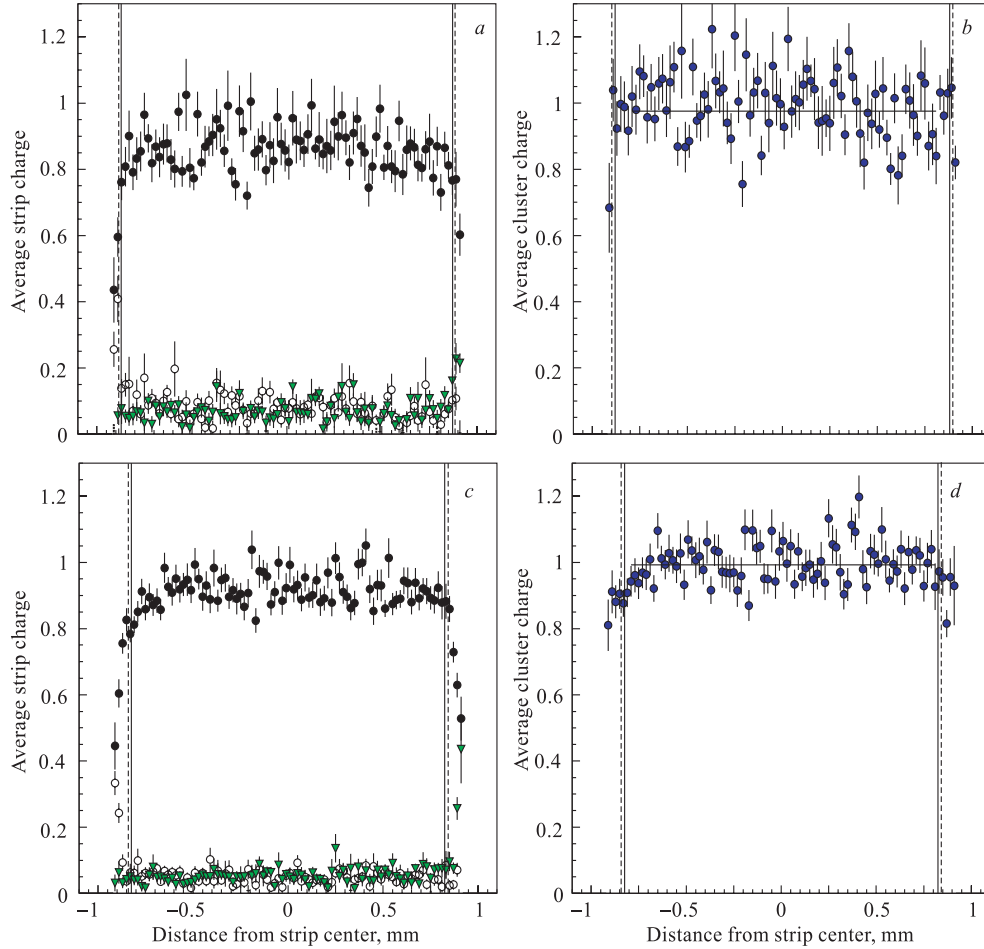


Fig. 16. Average strip (*a,c*) and cluster (*b,d*) charges as functions of the distance to the center of the central strip for Taiwan 45 at 400 V, small (*a,b*) and large (*c,d*) interstrip sections

One observes that:

1. There is a clear charge loss on the strip edge regions if the bias is below the efficiency plateau. This is the case for Hamamatsu 8 at 40 V (Fig. 20, *b*), Elma D2-1-n⁺ at 150 V (Fig. 21, *b*) and even more for Demokritos N5 (Fig. 22, *b*), which is thick and never reaches a good plateau.
2. Once on efficiency plateau, the cluster charge is always very uniform inside the implant region (Figures 13 to 19).
3. In the interstrip region one observes however even at high bias a small loss. This effect seems less pronounced if the distance between the Al lines is small (compare for

example Figs. 16, *a* and *c* which show the small and large interstrip regions of Taiwan 45 at 400 V).

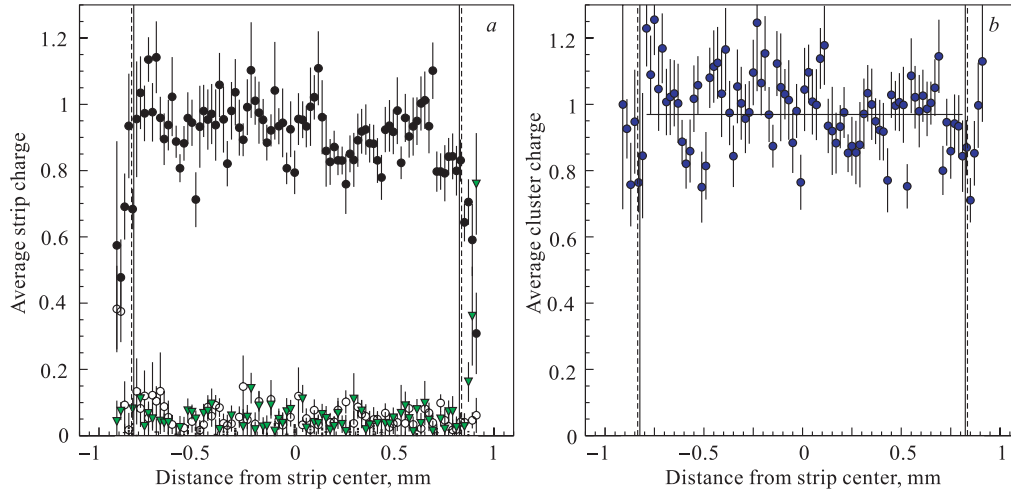


Fig. 17. Average strip (*a*) and cluster (*b*) charges as functions of the distance to the center of the central strip for Takion 3 at 500 V, large interstrip section

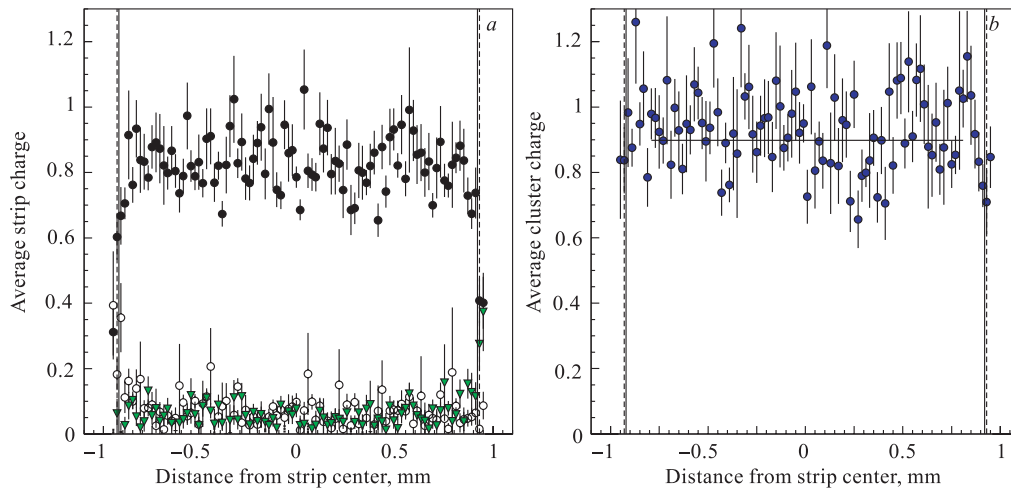


Fig. 18. Average strip (*a*) and cluster (*b*) charges as functions of the distance to the center of the central strip for Elma N9-1 at 450 V

To better quantify the last statement we have constructed the cluster charge distribution separating the data of each detector in only two sets (events inside or outside the implant

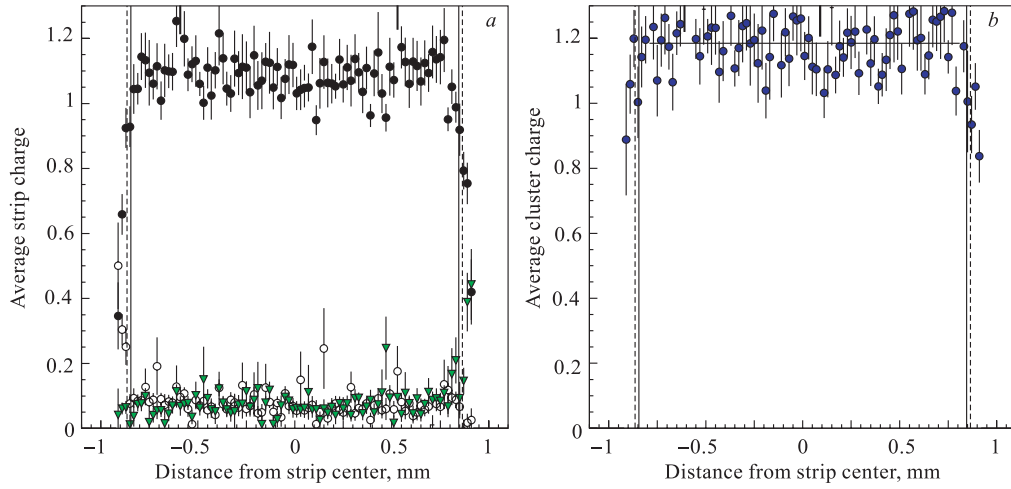


Fig. 19. Average strip (*a*) and cluster (*b*) charges as functions of the distance to the center of the central strip for Elma DSP7 at 650 V

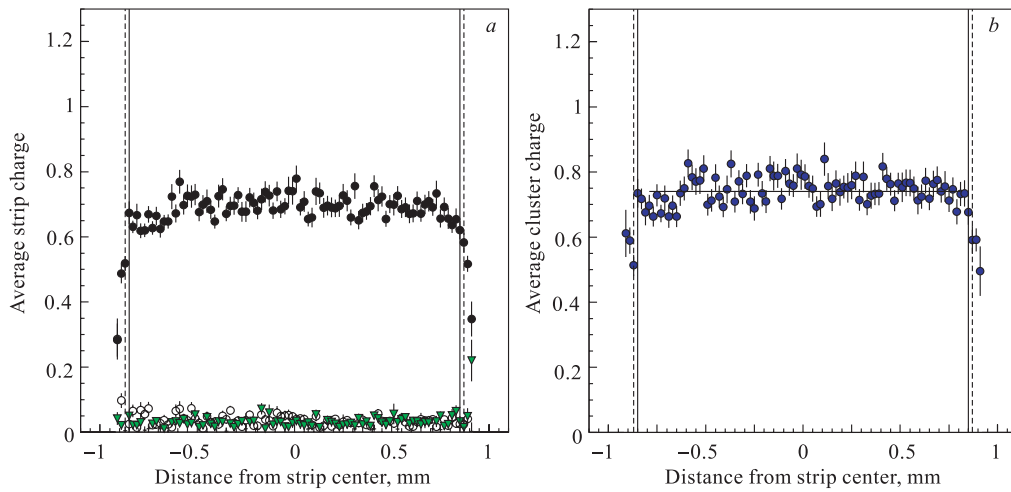


Fig. 20. Average strip (*a*) and cluster (*b*) charges as functions of the distance to the center of the central strip for Hamamatsu 8 at 40 V

region) and we plotted the ratio of either their most probable value or their average, the latter being more convenient in the case of small statistics. The most probable value is obtained through a local Gaussian fit of the maximum of the distribution.

When trying to compare the two regions, there is a difficulty in the definition of the cluster. We have used two possibilities:

- a 3-strips cluster centered around the central strip for the case where the particle hits inside the implant and a 2-strips cluster (one on each side) for an impact in the interstrip

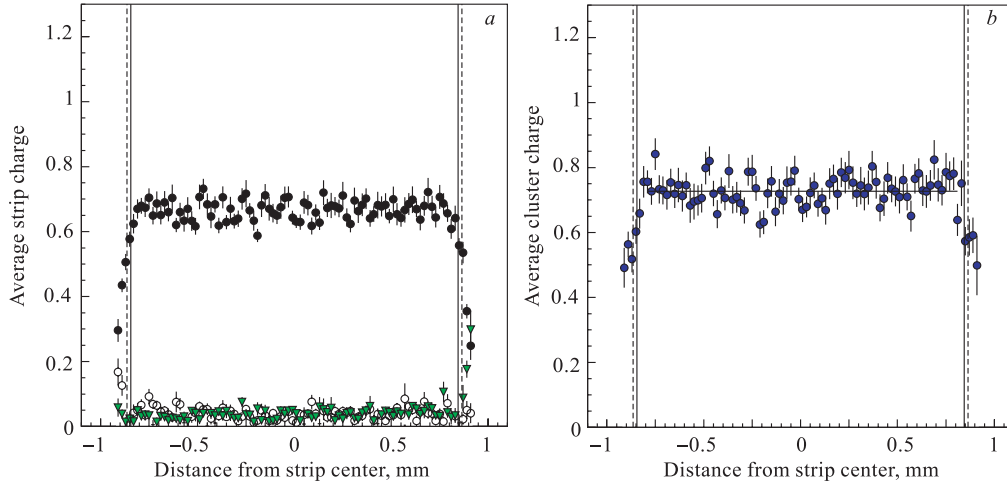


Fig. 21. Average strip (*a*) and cluster (*b*) charges as functions of the distance to the center of the central strip for Elma D2-1-n⁺ at 150 V

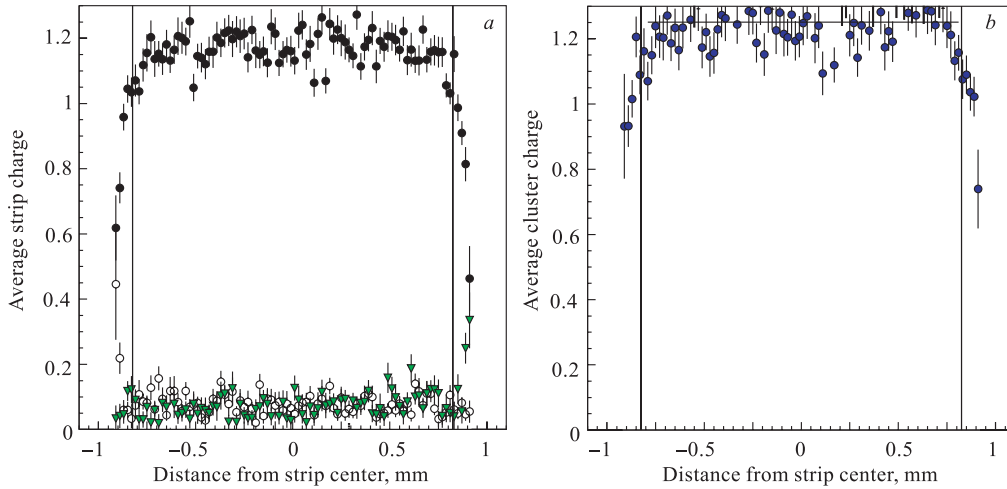


Fig. 22. Average strip (*a*) and cluster (*b*) charges as functions of the distance to the center of the central strip for Demokritos N5 at 600 V

region. This choice is very logical but may introduce a systematic difference between the two cases.

- a 4-strips cluster for both cases, which is a more symmetric definition. In the case of the central impact, the fourth strip is the nearest to the particle impact.

Figs. 23, *a,b,c* show the results as a function of the $p^+ - p^+$ distance for several detectors.

There is an effect in all cases. For a $p^+ - p^+$ distance of $50 \mu\text{m}$ the charge is practically independent of the position. For large gaps, as much as 15 % charge can be lost in the region between the implants. Electron showers have a very narrow spatial distribution: for example, an average of 32 % of the energy is deposited in a $95 \mu\text{m}$ wide region for a 120 GeV electron after $2X_0$ [1]. Therefore a charge loss in the interstrip region can introduce a nonnegligible spatial nonuniformity in the detector response if the interstrip region is too large. This effect has to be considered in the sensor specifications.

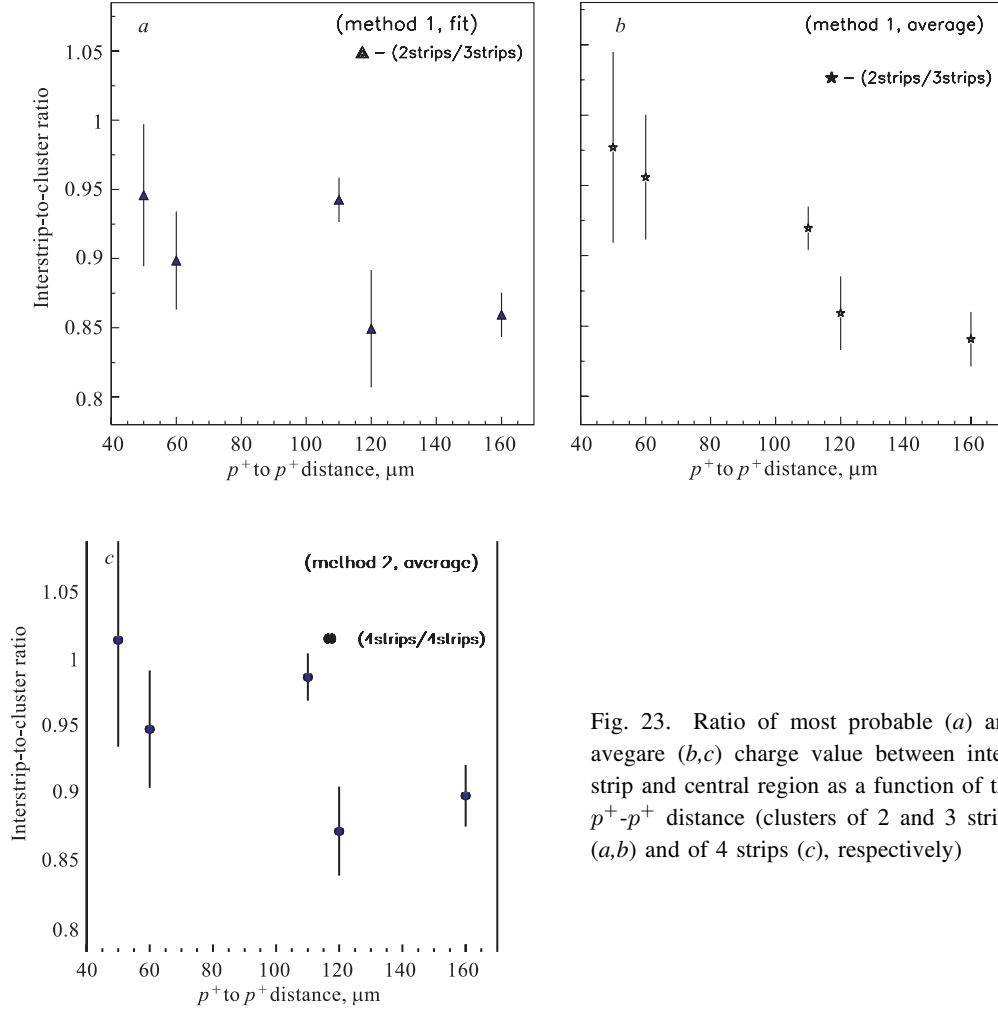


Fig. 23. Ratio of most probable (a) and average (b,c) charge value between interstrip and central region as a function of the $p^+ - p^+$ distance (clusters of 2 and 3 strips (a,b) and of 4 strips (c), respectively)

7.2. Cross-Talk. As can be seen on Figures 13–19, a, the charge on the left and right neighbour strips is not vanishing but has an average level of the order of 5 %, irrespective of the particle position. This effect is not due to an electronics cross-talk (we checked it

without detector), but to the interstrip capacitance. This explanation is sustained by Fig. 24, which shows that the fractional charge observed in the neighbour strip decreases with increasing interstrip distance. For the next two neighbours, the induced charge is very small (typically $\leq 0.5\%$).

7.3. Charge Collection Near the Guard Ring. Figure 25 shows the average charge as a function of position for the guard ring region of two detectors, Demokritos N5 and Taiwan 45-5, running both along (x) or across (y) the strips. The shape is the same in both directions. The charge collection extends to the guard ring region, being still 50 % 300 μm away from strip edge. This effect increases slightly the active area of the detector. Figure 26 shows the charge distribution in the guard ring region as a function of bias voltage. On the efficiency plateau the effect is independent of bias.

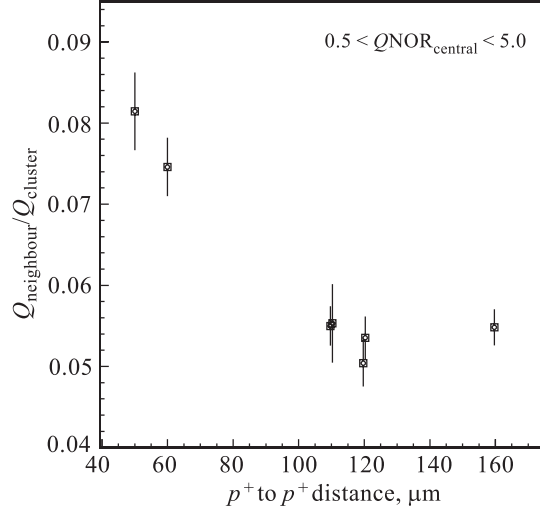


Fig. 24. Fraction of charge in the neighbour strip versus interstrip distance

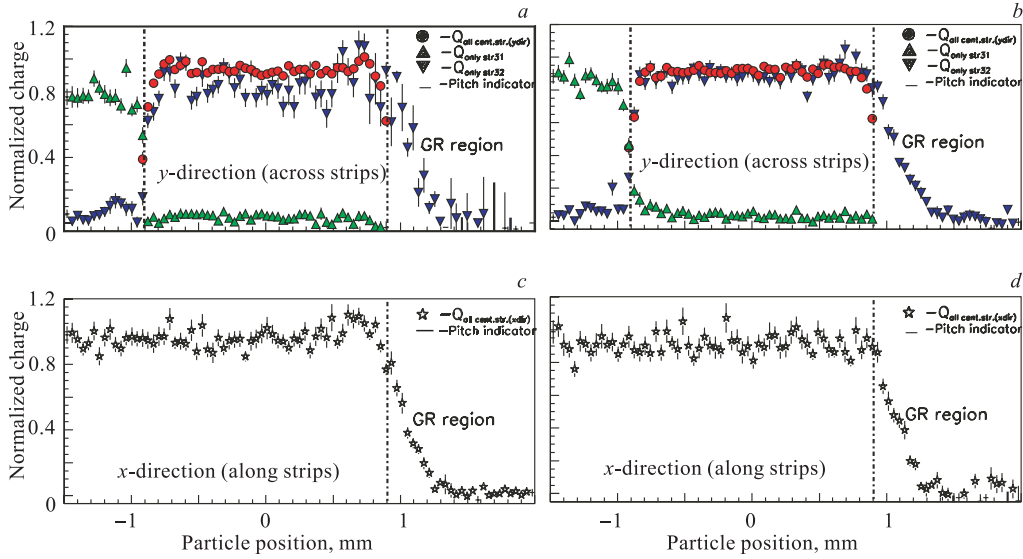


Fig. 25. CCE versus particle hit position for y - and x -direction for Demokritos N5 (a,c) and for Taiwan 45-5 (b,d)

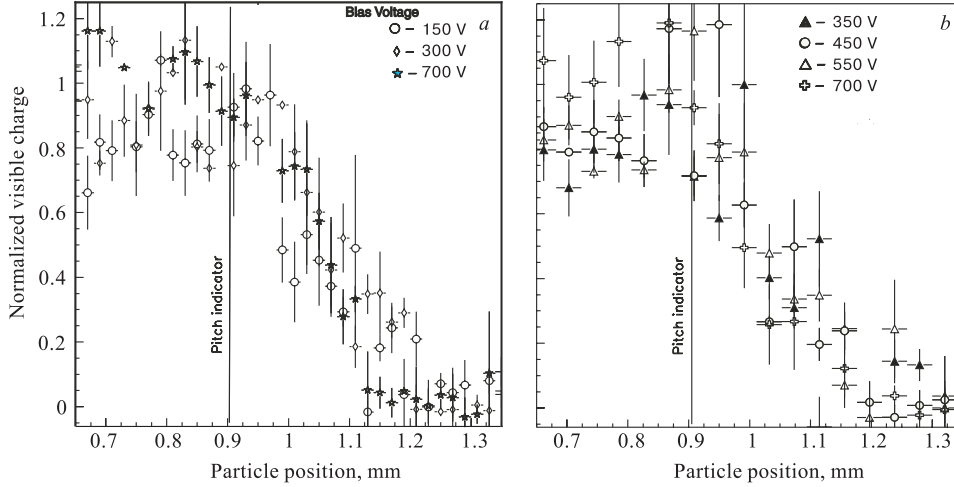


Fig. 26. CCE versus particle hit position for x -direction by different bias voltage for Hamamatsu 15 (a) and Taiwan 45-5 (b)

8. SIGNAL-TO-NOISE RATIO

We have measured a signal-to-noise ratio for various detectors on efficiency plateau. It is defined as the ratio of the central strip charge to the strip noise. The measurements are reported in Table 2. Due to the nonuniformity of the electronics, there are fluctuations from channel to channel (see Fig. 27) and a systematic error of ± 0.5 should be quoted for these values. The irradiated detectors have a signal-to-noise ratio close to 6, except for the thicker ones which have, as expected, a better performance.

Table 2. Signal-to-noise ratio

Detector	Bias voltage, V	S/N	Fluence $\cdot 10^{14} \text{ cm}^{-2}$	Thickness, μm
Hamamatsu 8	500	6.5	0	313
Taiwan 45-5	400	6.0	3.1 <i>p</i>	338
Hamamatsu 15	700	6.5	1.2 <i>n</i>	311
Elma N9-1	450	5.6	3.2 <i>p</i>	300
Elma D2-1-n ⁺	300	6.0	1.2 <i>n</i>	308
Elma DSP7	600	7.5	2.3 <i>n</i>	382

We recall that the SCT32 chip is not optimized for our large capacitance detectors. The expected SCT noise is $\sim 3400 e^-$ for the 60×60 mm detectors whose total capacitance/strip is around 44 pF and $\sim 3800 e^-$ for the 63×63 mm detectors whose capacitance is 50 pF [7]. The mip signal for a 300 μm thick detector is 25000 e^- . Taking into account the loss of the charge in the neighbour strips, we expect a signal-to-noise ratio of 6.6 (respectively 5.9) for small (respectively large) sensors at 100% charge collection efficiency. Our results are in agreement with these expectations.

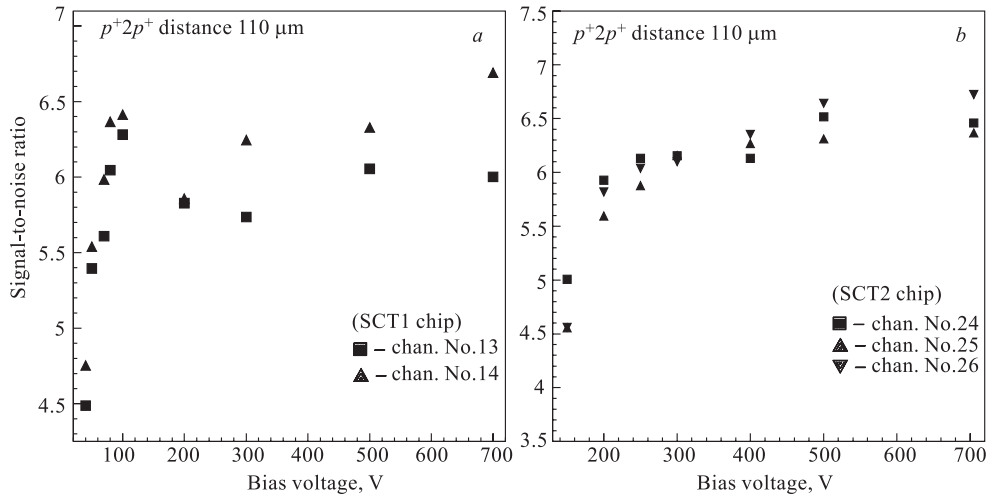


Fig. 27. Distribution of the signal-to-noise ratio versus bias voltage of the selected readout strip for Hamamatsu 8 (a) and Hamamatsu 15 (b)

Figure 27, *a, b* shows the evolution of the signal to noise ratio for Hamamatsu 8 (non-irradiated) and Hamamatsu 15 (irradiated) with bias voltage. There is no indication of a deterioration at very high bias values. Figure 28 shows the signal-to-noise ratio for the two geometry options of the Taiwan detector. At 400 V bias, the average signal-to-noise ratio is 6.05 in the 50 μm interstrip distance region and 6.35 in the 160 μm interstrip distance region. However, due to the large channel-to-channel nonuniformity, it is hard to draw a firm conclusion.

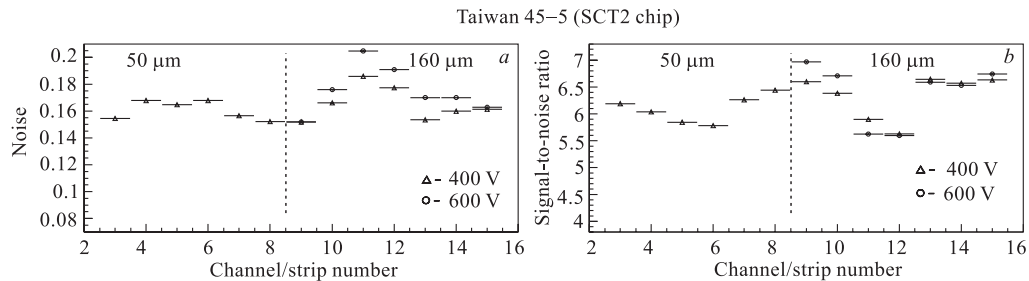


Fig. 28. Noise (a) and signal-to-noise ratio (b) as a function of the channel/strip number. The dotted line shows the boundary between the regions with different p^+ to p^+ distance

CONCLUSIONS

Thanks to the high precision telescope, details of the charge collection efficiency have been studied for irradiated detectors. The results agree with previous results obtained in the

laboratory with a radioactive source set-up. In all the cases, we found working conditions with high charge collection efficiency. The charge collection in the interstrip region increases for decreasing interstrip distances, yielding better spatial uniformity for small distances. However in this case the interstrip capacitance (and therefore both the noise [6] and the cross-talk with neighbour strips) increases for smaller distances. These two effects have to be compromised in the final specification.

Acknowledgements. We are thankful to P.V.Moissenz for his useful constructive discussion and remarks to the data processing. We are also grateful to V.V.Golikov and E.N.Kulagin for their contributions to this work as irradiation with fast neutrons and monitoring.

REFERENCES

1. Peisert A. et al. Silicon Detectors for the CMS Preshower. CMS NOTE-2000/061.
2. Bloch Ph. et al. Performance Study of Nonirradiated Prototype Silicon Preshower Samplers for CMS. CMS TN/2000-042.
3. Toker O. et al. // Nucl. Instr. Meth. A. 1994. V.340. P.572; manufacturer: IDE AS, Gaustadalleen 21, N-0371. Oslo., Norway.
4. Anghinolfi F. et al. SCTA — A Rad-Hard BiCMOS Analog Readout ASIC for ATLAS Semiconductor Tracker // IEEE Trans. Nucl. Sci. 1997. V.44, No.3 P.298–302.
5. Cheplakov A. et al. Radiation Hardness of GaAs Preamplifiers for Liquid Argon Calorimetry at LHC. MPI Report, PhE/96-15.
6. HBOOK, Reference manual. Program library Y250. Geneva: CERN, 1995.
7. Go A., Peisert A. Measurement of the Capacitance of Preshower Detectors. CMS IN-2000/041.

Received on March 28, 2001.